Materials Advances

ROYAL SOCIETY
OF **CHEMISTRY**

PAPER
Vincent Lapinte, Sebastien Blanquer *et al.*
4D printing of hydrogels based on poly(oxazoline) and
poly(acrylamide) copolymers by stereolithography

PAPER

Check for updates

4D printing of hydrogels based on poly(oxazoline) and poly(acrylamide) copolymers by stereolithography†

Thomas Brossier,‡[ab] Michel Habib,‡[a] Belkacem Tarek Benkhaled,‡[a] Gael Volpi,[b] Vincent Lapinte [ID] *[a] and Sebastien Blanquer [ID] *[a]

Programmed shape deformation of hydrogels by thermal stimulation has great potential due to the remarkable possibilities of 4D printing process in a wide domain of applications. Consequently, high requests are dedicated to the synthesis and study of smart hydrogels for additive manufacturing. This work revolves around the synthesis of two new thermo-responsive hydrogel systems based on copolymers of poly(oxazoline) and poly(acrylamide). For each system, the thermo-sensitive part corresponds to poly(2-isopropyl-2-oxazoline) (PiPrOx) or poly(N-isopropylacrylamide) (PNIPAM), while the crosslinking is carried by the poly(oxazoline) comonomer blocks. Photocrosslinked resin is obtained during the stereolithography (SLA) printing process leading to different macromolecular networks and properties. The volume transformation of the hydrogels is evaluated by the measurement of water content at different temperatures in order to estimate the sorption's kinetics and to determine the volume phase transition temperature (VPTT). The impact of the VPTT on each hydrogel system is highlighted by their mechanical properties. Finally, 3D porous structures, based on these thermo-responsive hydrogels, are manufactured by 4D SLA printing and the shrinking/expansion effects with the temperature change are illustrated.

1. Introduction

Smart hydrogels, defined as stimuli-responsive polymeric networks, are able to change their morphology or properties in response to chemical (pH, ionic interactions), physical (temperature, light, electromagnetic) or biological (enzymatic interactions) stimulations. Such unique properties have gained promising potential not only for academic research but also in various domains of applications such as in biomedicine, robotics, or electronics.[1–5]

In the last decade, the interest in these smart materials has gained more attention with the combination of stimuli-responsive hydrogels and additive manufacturing leading to

4D printing. 4D printing is an exciting emerging technology where 3D printed structures can be programmed to change their form, properties or functions over time in response to an external stimulus.[6] Dynamic 4D printed hydrogels have the ability to physically reconfigure their volume in response to external triggers allowing them to adapt to their environment. Among all the stimulation types, the most common and relevant approach to generate shape-morphing in 4D printed hydrogels is temperature control.[7,8] Thermal-stimulation has the advantage to obtain a fast and reversible deformation without needing a chemical treatment. Traditionally, these smart hydrogels are based on thermo-sensitive polymers that display a critical temperature of solubility in water (upper or lower critical solution temperature UCST/LCST).[9] Crosslinking these thermo-sensitive polymers leads to thermo-responsive hydrogel systems. The characteristic UCST/LCST of the polymer will be translated to a volume phase transition temperature (VPTT) describing the reversible water expulsion or absorption from the polymer matrix. More precisely, upon stimulation, the polymer chains undergo a change in their conformation which can favor either polymer–water interactions (swelling effect) or polymer-polymer interactions (shrinking effect).[10]

Even though thermo-responsive networks have considerable potential, the number of used smart-materials is still limited. In

[a] ICGM, University of Montpellier, CNRS, ENSCM, Montpellier, France.
E-mail: sebastien.blanquer@umontpellier.fr

[b] Marle-3D Medlab Marignane, France

† Electronic supplementary information (ESI) available: Table storage modulus and calculated mesh size; ^{1}H NMR spectra of HDOTs, PMOx, PiPrOx; swelling pictures of the hydrogels; mesh size calculation; details on the PiPrOx$_{20}$-*net*-PAM$_{100}$ properties; diffusion water curves using Ritger-Peppas model; picture of the 4D printed device; Movies S1 and S2 of the mechanical handling of the hydrogels; Movie S3 of the swelling effect of 4D printed device based on PiPrOx$_{20}$-*net*-PAM$_4$. See DOI: https://doi.org/10.1039/d3ma00665d

‡ These authors contributed equally to this work.
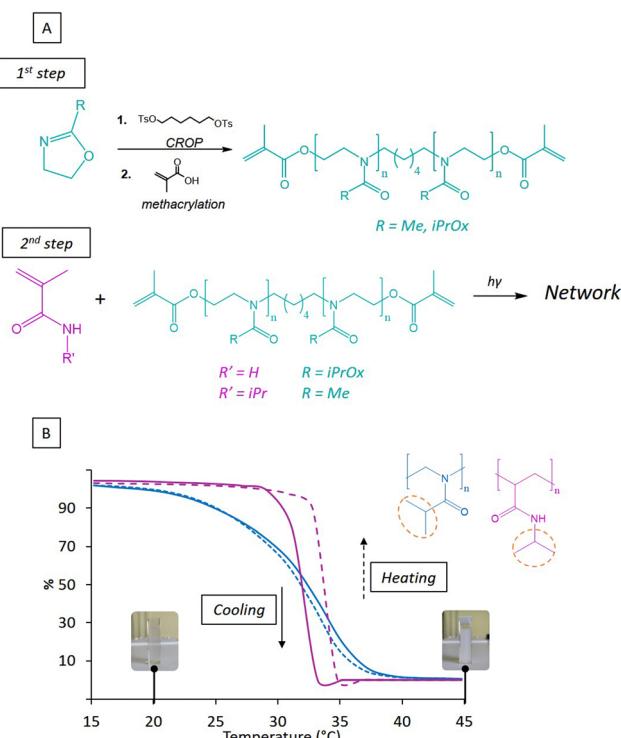
Fig. 1 (A) Synthesis of the hydrogels based on copolymers PMOx-*net*-PNIPAM and PiPrOx-*net*-PAM, B/UV-Transmittance of solution of PNIPAM (violet lines) and PiPrOx (blue lines) (0.5 mg mL^{-1}) related to temperature by using UV spectroscopy. Heating cycle (dotted line) and cooling cycle (full line) (2 °C min^{-1}). Pictures represent the PiPrOx at 20 °C, and PiPrOx at 45 °C (same behavior has been obtained for PNIPAM).

the literature, copolymers based on poly(N-isopropylacrylamide) (PNIPAM) remains the gold standard of thermo-sensitive smart hydrogels, especially due to its convenient LCST around 32–35 °C in water.[11,12] Once coupled with a crosslinking agent, the generated PNIPAM based matrix exhibits a reversible volume change. Basically, in water, the hydrogel swells below the volume phase transition temperature and collapses above it. Such volume transformation close to physiological temperature becomes attractive for biomedical applications.[13,14] However, due to the neurotoxicity of the NIPAM monomer, several studies orient their research towards new biocompatible thermo-responsive hydrogels.[15] In this perspective, the poly(oxazoline) (POx) family has a particular interest especially in the biomedical field and 3D printing hydrogels.[16–21] In addition, their properties can be modulated by changing the R substituent of the monomer (Fig. 1) leading to material with a LCST ranging from 20 to 80 °C.[22] Among the thermo-sensitive POx, poly(2-isopropyl-2-oxazoline) (PiPrOx) bearing an isopropyl group similarly to PNIPAM has a LCST around 35 °C.[23–25] Nevertheless, PiPrOx has been barely used as a thermo-responsive hydrogel. Li *et al* studied PiPrOx based copolymers and determined a significant impact on the volume change under cooling and heating procedure.[24] Then recently, Madau *et al* coupled PiPrOx with hyaluronic acid to generate a thermo-sensitive biomaterial with volume phase transition

temperature around 36 °C.[26] Besides these studies no more investigation of POx based thermo-responsive systems has been reported and their use in 4D printing process is still unstudied. Meanwhile, the elaboration of 3D printed structures with high resolution and having the ability to deform in response to thermal-stimulation remains highly challenging. From the literature, few works have been reported on stimulated hydrogels fabricated by additive manufacturing. Han *et al* reported the first 3D printed thermo-sensitive hydrogel using μ-stereolithography and showed the impact of the crosslinker to NIPAM ratio monomer on the VPTT.[27] More recently, Guo *et al* used a hybrid polymer based on agarose and poly(acrylamide) to induce deformation of 3D extruded structures, given the thermogelation of agarose around 35 °C.[28] Besides these articles, most of the studies involving 4D printed hydrogels are generally limited to basic bilayers actuators.[17,29–31]

Therefore, we propose in this study to investigate 4D printed structures by the stereolithography approach using thermo-sensitive hydrogels based on acrylamide and oxazoline copolymers. Regarding the thermo-sensitive property, it will be provided by the acrylamide (PNIPAM) segments for the first system and oxazoline (PiPrOx) segments for the second system as a non-toxic thermo-responsive substituent.[19,32]

2. Experimental section/methods

Material

2-Methyl-2-oxazoline (MOx, Sigma Aldrich, 99.0%), 2-isopropyl-2-oxazoline (iPrOx, Sigma Aldrich, 99.0%), 1,6-hexanediol (HD, Sigma Aldrich, 99.0%), methacrylic acid (MAA, Alfa Aesar, 99.0%), triethylamine (TEA, Sigma Aldrich, 98.0%), anhydrous acetonitrile (Sigma Aldrich, 99.9%), *p*-toluenesulfonyl chloride (TsCl, Sigma Aldrich, 99.0%), methacrylic anhydride (Sigma Aldrich, 94%), orange G (Sigma Aldrich), 2-hydroxy-2-methylpropiophenone (Darocur 1173, Sigma Aldrich), N-isopropylacrylamide (NIPAM, Sigma Aldrich 97.0%), acrylamide (Acry, Sigma Aldrich, 99.0%), diethyl ether and ethylene glycol were commercial products and used without further purification.

Synthesis

Synthesis of 1,6-hexaneditosylate (HDOTs). To a 250 mL round-bottom flask equipped with a magnetic stir bar, 1,6-hexanediol (HD) (10 g, 0.85 mol) and TEA (57 mL, 4.25 mol) were dissolved in 100 mL of chloroform. The solution was cold at 0 °C and TsCl (65 g, 3.4 mol) was added dropwise. The resulting mixture was stirred overnight at 25 °C. The crude was washed with water and 3 times with dichloromethane. The organic phase was concentrated and stored in fridge until crystallization. The compound was recrystallized with ethanol and a white solid product was isolated in 75% yield.

^{1}H NMR (CDCl$_3$), δ (ppm): 7.7 (d. 4H, H2), 7.3 (d, 4H, H2), 3.9 (t, 4H, H3), 2.5 (s, 6H, H1), 1.6 (m, 4H, H3) et 1.3 (m, 4H, H3) (Fig. S1, ESI†).

Synthesis of bis-methacrylated poly(2-methyl-2-oxazoline) (PMOx$_{20}$). To a 500 mL round-bottom flask equipped with a

magnetic stir bar, HDOTs (11 g, 0.029 mol) was dissolved in 300 mL of anhydrous acetonitrile and MOx (49.5 mL, 0.588 mol) were added. The solution was vigorously stirred at 80 °C for 4 h. The resulting polymer was then quenched by the dropwise addition of TEA (27 mL, 0.196 mol) and methacrylic acid (13 mL, 0.714 mol). The flask was maintained at 40 °C for 15 h. After cooling, the reaction mixture was concentrated, then precipitated in diethyl ether and dry under pressure. A solid powder was obtained with a yield of 93%.

^{1}H NMR (CDCl$_3$) δ (ppm): 6.08 (1H, H2), 5.61 (2H, H2), 4.26 (2H, H3) 3.20–3; 66 (4H, H4), 2.01–2.21 (3H, H5), 1.91 (3H, H1), 1.20–2.41 (8H, H6) (Fig. S2, ESI†).

Synthesis of bis-methacrylated poly(2-isopropyl-2-oxazoline) (PiPrOx$_{20}$). In a 20 mL vial equipped with a magnetic stirring bar, HDOT (0.94 g, 2.2 mmol) and iPrOx (5 g, 44 mmol) were dissolved in 10 mL of anhydrous acetonitrile. The vial was put in the microwave reactor for 17 min at 135 °C under a power of 200 W. The resulting polymer was transferred to a 100 mL flask. Then, the polymerization was completed by the dropwise addition of TEA (0.8 mL, 11 mmol) and methacrylic acid (0.76 mL, 8.8 mmol). The solution was kept at 40 °C for 15 h. After cooling, the reaction mixture was concentrated, precipitated in diethyl ether and dried under vacuum. A solid powder was obtained in 96% yield.

^{1}H NMR (CDCl$_3$) δ (ppm): 6.08 (1H, H2), 5.54 (2H, H2), 4.22 (2H, H3) 3.12–3.63 (4H, H4), 2.55–2.89 (1H, H5), 1.86 (3H, H1), 0.96–1.12 (6H, H6), 0.91–1.69 (8H, H7) (Fig. S3, ESI†).

Photo-sensitive resins formulation for SLA fabrication. To prepare the resin formulations for stereolithography, the polymers were mixed with ethylene glycol (33 wt% of the resin) as a non-reactive diluent. Liquid TPO (3 wt% relative to the polymer) and Orange G (0.2 wt% relative to the polymer) were added as photoinitiator and coloring agent respectively.

Characterization

Nuclear magnetic resonance (NMR) spectroscopy. ^{1}H NMR spectra were recorded on a 400 MHz Bruker Aspect Spectrometer. CDCl$_3$ was used as deuterated solvent. Chemical shifts were given in parts per million (ppm). For ^{1}H NMR the residual CHCl$_3$ in CDCl$_3$ at 7.26 ppm was considered as reference peak. The molar mass of polymers (POx) was determined using the following eqn (1) and (2):

$$\mathrm{DP}_n(\mathrm{POx}) = \frac{\frac{\int_{3.2}^{3.8} I}{8}}{\frac{\int_{5.7}^{6.1} I}{4}} \tag{1}$$

$$M_{n,\mathrm{NMR}} = \mathrm{DP}_n(\mathrm{POx}) \times M_{\mathrm{Ox}} + 2 \times M_{\mathrm{methacrylate}} \tag{2}$$

where M_{Ox} and $M_{\mathrm{methacrylate}}$ are the molar masses of repetitive units ($M_{\mathrm{MOx}} = 85$ g mol^{-1} and $M_{\mathrm{iPrOx}} = 113$ g mol^{-1}) and methacrylate end chain ($M_{\mathrm{methacrylate}} = 86$ g mol^{-1}).

Size exclusion chromatography (SEC). The number of average molecular weights and dispersity of the polymers were determined using a SEC system (PL-GPC 50 Plus) equipped with an autosampler (Varian model 410). (The apparatus consists of a refractive index detector, a PolarGel-M precolumn and a precolumn PolarGel-M (7.5 $\times$ 50 mm), and two columns PolarGel-M (7.5 $\times$ 300 mm) thermostated at 50 °C. The mobile phase is N,N-dimethylacetamide (DMAc) (with 0.1 wt% LiCl) at a flow rate of 0.8 mL min^{-1}, calibrated with poly(methyl methacrylate) (PMMA) standards ranging from 550 to 2 000 000 g mol^{-1} (EasiVial-Agilent).

Differential scanning calorimetry (DSC). DSC analyses were carried out using a Mettler Toledo (Mettler Toledo, France) DSC1 calorimeter. A constant calibration was performed with standards of biphenyl, indium, bismuth, zinc, and cesium chloride standards Nitrogen was used as the purge gas. An amount of swelled gels ($Q\%$ = 150–200%) were put in Aluminum standard 40 µl sample holder. Thermal properties were recorded between 0 and 60 °C at a heating rate of 5 °C min^{-1}. For the measurements, in order to detect a signal in DSC the samples were not analyzed in the equilibrium state but in a semi-swollen state with 50 wt% water.

Mesh size and rheology. All tests were done on a Thermo Fisher HAAKE MARS 60 rheometer using 8 mm parallel circular sanded plate-plate geometry. The samples used were cylindrical disks of 8 mm diameter and 1 mm thickness similar to the plates' diameter and the fixed gap value respectively. Frequency sweeps were done between 1 and 10 rad s^{-1} in the linear viscoelastic domain at a constant 1% strain at 20 °C.

Cross-linking density was evaluated by calculating the mesh size ξ (Å) using eqn (3):[33,34]

$$\xi(\text{Å}) = 10^{10} \times \sqrt[3]{\frac{G' \times N_A}{R \times T}} \tag{3}$$

Where ϑ_e is the specific volume of the mesh in m^{-3}, G' is the storage modulus in the linear regime in Pa, N_A Avogadro's number, R gas constant and T the temperature at which G' was measured (293 K). Mesh size was calculated assuming a cubicic unit between the crosslinking points. The results are shown in Table S1 (ESI†).

Mechanical testing. Hydrogel compression tests were performed on an Instron 3366L5885 instrument. Cylindrical samples of 10 $\times$ 5 mm were prepared by stereolithography and immersed in water for 2 days before testing. The compression was performed at a speed of 5 mm s^{-1}. The compressive strain was expressed as a percentage of the length. Each point represents the mean $\pm$ standard deviation ($n = 3$).

Gel content and water uptake. Photo-crosslinking efficiency was calculated by gel content on cylindrical samples of 10 $\times$ 5 mm prepared by stereolithography and immersed in water for 2 days before testing. The samples were first wiped after fabrication and then weighed to obtain the initial mass (m_i). Then, the samples were immersed in distilled water for 48 h (the water was renewed five times a day). After washing, the polymers were dried under a vacuum to determine the dry weight (m_d). The gel content was determined according to eqn (4):

$$\text{gel content} = \frac{m_d}{m_i} \times 100 \tag{4}$$

The water uptake (Q), kinetics of the hydrogels was calculated from the swollen mass (m_s) and dry mass (m_d). The hydrogels

were immersed in distilled water at room temperature or 50 °C. Hydrogels were weighed every hour from 1 to 8 h and then after 15, 24 and 48 h to determine m_s. Hydrogels were dried under vacuum to deduce m_d. Equilibrium water uptake was calculated with the masses at 48 h. The kinetics of water uptake of water was calculated as following eqn (5):

$$Q = \frac{m_s - m_d}{m_d} \times 100 \quad (5)$$

Determination of the diffusion mechanism with Ritger–eppas model. The behavior of water transport and the swelling kinetic of the hydrogels were investigated by using the Fickian diffusion model represented by eqn (6) and (7) (considering only the data fulfilling the condition $SD_t/ESD \leq 0.6$).

$$\frac{m_t}{m} = \frac{SD_t}{ESD} = k \cdot t^n \quad (6)$$

$$\log \frac{SD_t}{ESD} = n \cdot \log(t) + \log(k) \quad (7)$$

Where k is a characteristic of both gel and solvent and n the swelling exponent, indicating the diffusion mechanism. The plots of $\log(SD_t/ESD)$ versus $\log(t)$ were depicted to determine n and k.

k corresponds to $\log(SD_t/ESD)$-intercept and n the slope of the curve. Depending on the relative rates of diffusion and polymer relaxation, three mechanisms can be distinguished: (i) Fickian diffusion mechanism (case I) when $n = 0.5$, (ii) non-Fickian (anomalous) diffusion mechanism for $0.5 < n > 1$, and (iii) case II diffusion mechanism when $n = 1$.

Fabrication of 3D printed object by SLA. Three-dimensional cubic porous structures with 1 mm walls were designed using the STL format of Rhinoceros 3D. The 3D structures were constructed from the mentioned resins by stereolithography using a digital light processing (DLP) machine (Max X27, Asiga Australia) with a 385 nm wavelength. The 3D objects were constructed by photo-crosslinking successive layers of resin with a thickness of 100 μm. Each layer was irradiated at an intensity of 20 mW cm^{-2} for 30 s. After construction, the structures were washed in distilled water for 48 h while changing the water twice a day.

3. Results and discussions

The design of a thermo-responsive 4D hydrogel system is done by incorporating either NIPAM or PiPrOx in the matrix. To ensure a mechanically strong enough hydrogel to be printing under stereo-lithography process, the hydrogel precursors consist of acrylamide monomers and POx macromonomer also acting as crosslinker. Besides the thermal-response that can be added, these copolymers are chosen because of their specific hydrogen bond interactions. In fact, the mechanical properties of the crosslinked network will be improved due to the interactions between the hydrogen bonds acceptor from the POx blocks and hydrogen bonds donor from the polyacrylamide blocks.[35] This particular improvement in the mechanical properties will facilitate the stereolithography printing process of the hydrogels, given that the challenging aspect of 3D printing of hydrogels is their weak mechanical properties.[18]

3.1. Macromonomer synthesis

The prepared hydrogels are based on commercial acrylamide (AM) or N-isopropylacrylamide (NIPAM) monomers and POx macromonomer also acting as crosslinker. The POx comonomers, which includes PiPrOx and poly(2-methyl-2-oxazoline) (PMOx) have been synthesized (Fig. 1B) in a one pot step via cationic ring-opening polymerization (CROP) using 2-methyl-2-oxazoline (MOx) and 2-isopropyl-2-oxazoline (iPrOx) monomers respectively. CROP initiation was occurred by using synthesized 1,6-hexaneditosylate, a highly reactive electrophilic difunctional initiator (Fig. S1, ESI†). CROP of MOx monomer was processed under conventional conditions while iPrOx was polymerized under microwave given its low reactivity. PiPrOx and PMOx were characterized by ^{1}H NMR spectroscopy (Fig. S2 and S3, ESI†). Finally, the polymerization was completed by in situ terminal methacrylation in presence of methacrylic acid, in order to generate a photosensitive resin as previously reported.[18] The reaction scheme of each synthesis is presented in Fig. 1A.

3.2. Thermo-sensitivity of homopolymers PiPrOx and PNIPAM

Even though polymers based on poly(acrylamide) are widely investigated to build thermo-sensitive hydrogel systems, only few studies report the use of poly(oxazoline) for smart hydrogels. However, POx is becoming a class of polymers in a considerable expansion, especially for its water-solubility leading to hydrogels or to nanomaterials for drug delivery.[36,37] Moreover, the generation of POx hydrogels able to display morphological change near body temperature is of great interest for biomedical applications. Hence, prior to any hydrogel preparation, we investigated first the thermo-sensitivity of the PiPrOx and PNIPAM homopolymers. To corroborate previous works from the literature regarding both LCST polymers, we monitored their thermo-stimulation by UV spectroscopy (Fig. 1B). PNIPAM was synthesized by free radical photo-polymerization and PiPrOx CROP using tosylate initiation. A total conversion was reached for both homopolymers, and cloud temperatures of 31 and 33 °C were detected for PNIPAM and PiPrOx respectively in agreement with the literature as seen.[23] In both cases, a turbidity of the solution appeared under heating as illustrated in Fig. 2A. The comparison of the absorbance evolution versus the temperature reveals two different behaviors between the polymers. In terms of kinetics of turbidity, it can be clearly noticed the rapid transition from solution to precipitation for PNIPAM ($\Delta T = 5$ °C) whereas the transition for PiPrOx is slower ($\Delta T = 20$ °C) due to the typical type I LCST phase behavior of PiPrOx by contrast to type II LCST of PNIPAM as previously reported by Zhao et al.[38] The relatively weaker hydrogen bonds in water of PiPrOx, which has only hydrogen acceptors, compared to PNIPAM, which contains secondary amine groups, provides an explanation for the variation in their facility to establish hydrogen bonds with water molecules. This distinction clarifies the minimal hysteresis observed in the case of homopolymer PiPrOx, in contrast to the pronounced thermal hysteresis obtained for PNIPAM. The low hysteresis observed for PiPrOx highlights the complete reversibility of interactions involving isopropyl groups, occurring with a similar kinetics due to

the weaker hydrogen bonds and the absence of polymer-rich phase vitrification at high temperature.

3.3. Thermo-sensitive hydrogels PMOx-*net*-PNIPAM and PiPrOx-*net*-PAM.

Once the LCST determined for both homopolymers, the hydrogels were obtained using the stereolithography process. Among the numerous additive manufacturing technologies, stereolithography (SLA) is recognized for its remarkable efficiency and several advantages in terms of versatility, high accuracy and processing speed. In addition, the 3D hydrogel structure is obtained layer by layer *via* photo-crosslinking. The network types created through stereolithography are denoted as PiPrOx-*net*-PAM and PMOx-*net*-PNIPAM in accordance with the IUPAC's recommendation for crosslinked copolymers, where "*net*" refers to network structure.

The amount of photoinitiator (TPO) and photoabsorber (Orange G) have been optimized at 3 and 0.2 w/w% respectively in order to obtain the best resolution and a short manufacturing time. It is well established that the LCST, and consequently the VPTT, of copolymers can be influenced by both the ratio of thermoresponsive units and the size of the thermoresponsive blocks. In our system, it won't be feasible to exert control over the photo-polymerization process, particularly in terms of regulating monomer insertion (including acrylamide or methacrylate from the modified POx); however, we do regulate the specified ratio of each component within the resulting network. Hence, for each system PiPrOx-*net*-PAM and PMOx-*net*-PNIPAM, two ratios of

POx/Am were evaluated to study the influence of the thermo-responsive moieties' amount on the thermo-sensitivity of the crosslinked system. The first formulation was chosen to have a 5 times molar excess of Am monomers while for the second formulation, the Ox moieties are in a 5 times molar excess. In doing so, the same ratio of thermo-sensitive units to the hydrophilic comonomer is respected for both generated hydrogel types. The exact formulations are shown in Table 1. In both strategies, the crosslinker is the POx (PiPrOx or PMOx) macromonomer bearing methacrylate end groups. The comonomer Am (PNIPAM or polyacrylamide (PAM)) improves the mechanical properties of the hydrogel's network due their strong interaction with the POx moieties. Two molar ratios 1/5 and 5/1 of POx/Am were tested for each formulation resulting in different macromolecular networks with different mesh sizes obtained by rheological measurements as illustrated in Fig. 2 and Table S1 (ESI†). It is important to note that for both cases, the thermo-sensitivity results from the balance between the hydrophilic amido groups and the hydrophobic isopropyl groups. Given that the POx macromonomer has a $DP_n = 20$, the designation of POx_{20}-*net*-PAM_{100} and POx_{20}-*net*-PAM_4 are chosen to represent both molar ratios 1/5 and 5/1 respectively. For all the hydrogels fabricated by SLA, the efficiency of the crosslinking was calculated using the gel content equation (eqn (4)), with values between 86 and 92% achieved.

The phase transition of the hydrogels has been visualized by a higher opacity and a notable shrinkage of the hydrogel, while the thermodynamic behavior was determined by DSC. In fact, sufficient energy must be consumed by the system at the LCST, in order to induce the dissociation between the amide groups and the water molecules which corresponds to an endothermic process detected by DSC analysis.[39,40] Therefore, from the DSC thermograms (Fig. 3), an endothermic peak is clearly identified for $PMOx_{20}$-*net*-$PNIPAM_{100}$ and $PiPrOx_{20}$-*net*-PAM_4 while no endothermic peak was detected for $PMOx_{20}$-*net*-$PNIPAM_4$ and $PiPrOx_{20}$-*net*-PAM_{100}. The absence of endothermic process can be explained by the excess of hydrophilic moieties PAM or PMOx with respect to the thermo-sensitive units represented by the PiPrOx or PNIPAM. It can be concluded that a molar ratio 5/1 of thermosensitive units to hydrophilic units is needed to observe a thermal response. The 4D study will focus on the two systems that follows the previously mentioned criteria, which are $PMOx_{20}$-*net*-$PNIPAM_{100}$ and $PiPrOx_{20}$-*net*-PAM_4.

Hence, for the thermo-sensitive systems, the maximum endothermal peak was associated to the VPTT, which was detected at 37 and 42 °C for $PMOx_{20}$-*net*-$PNIPAM_{100}$ and $PiPrOx_{20}$-*net*-PAM_4 respectively. It can be noticed a temperature
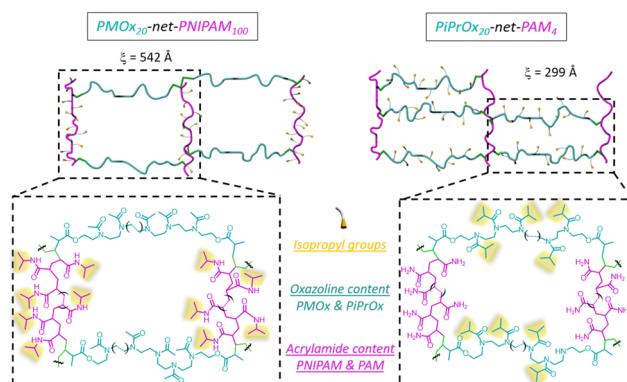
Fig. 2 Synthesis of the hydrogels based on copolymers $PMOx_{20}$-*net*-$PNIPAM_{100}$ (5/1) and $PiPrOx_{20}$-*net*-PAM_4 (5/1), and illustration of the resulting networks. Blue corresponds to POx blocks, purple for acrylamide units and green for methacrylate moieties.

Table 1 Description of photo-crosslinkable resins with molar ratio of each chemical agent (33 wt% of the resin)

Hydrogel	Molar ratio of Pox crosslinker *vs.* acrylamide monomer	PMOx or PiPrOx[a] (mmol)	Monomer (mmol)
$PMOx_{20}$-*net*-$PNIPAM_{100}$	1/5	8.85×10^{-2}	8.85
$PMOx_{20}$-*net*-$PNIPAM_4$	5/1	0.52	2.09
$PiPrOx_{20}$-*net*-PAM_{100}	1/5	0.14	14
$PiPrOx_{20}$-*net*-PAM_4	5/1	0.44	1.77

[a] PMOx ($DP_n = 20$, $M_{n\,NMR} = 2502$ g mol^{-1}, $M_{n\,SEC} = 4030$ g mol^{-1}, $Đ = 1.29$), PiPrOx ($DP_n = 20$, $M_{n\,NMR} = 1945$ g mol^{-1}, $M_{n\,SEC} = 3660$ g mol^{-1}, $Đ = 1.18$).
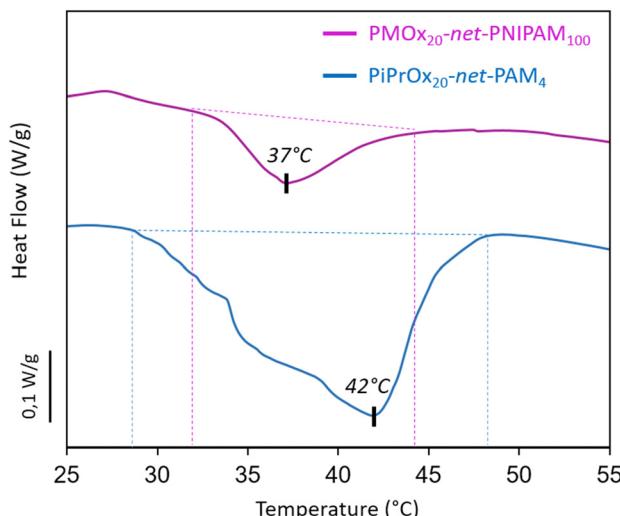
Fig. 3 Thermogram of hydrogels PiPrOx$_{20}$-*net*-PAM$_4$ and PMOx$_{20}$-*net*-PNIPAM$_{100}$ by using DSC (5 °C min^{-1}).

Fig. 4 Swelling kinetics in water at 20 and 50 °C and compressing tests of (A) and (B) PMOx$_{20}$-*net*-PNIPAM$_{100}$ and PMOx$_{20}$-*net*-PNIPAM$_4$ and (C) and (D) PiPrOx$_{20}$-*net*-PAM$_{100}$ and PiPrOx$_{20}$-*net*-PAM$_4$ (scale bar 5 mm).

shift to higher values for both crosslinked networks compared to the LCST of the homopolymers.[41] This can be attributed to the incorporation of hydrophilic segments within the network, as well as explained by a decrease in chain mobility following the crosslinking process, which slows down the phase transition with increasing temperature.[24] Moreover from the thermogram, PiPrOx$_{20}$-*net*-PAM$_4$ exhibits a thermal response starting at 29 °C and PMOx$_{20}$-*net*-PNIPAM$_{100}$ thermal response starts at 32 °C which can result in a phase transition with greater temperature range. This result can be correlated to the behavior of the thermo-responsive homopolymers, and can therefore be explained by the lower affinity of the PiPrOx to water compared to PNIPAM. Nevertheless, for both copolymers the shape-morphing effect can be expected to be done at 37 °C suitable for biomedical applications.

The influence of the temperature on the smart hydrogels was also evaluated by measuring the swelling kinetics at 20 °C and the shrinking at 50 °C by gravimetric method, using cylinders fabricated by SLA (Fig. 4). The swelling degree of each hydrogel was measured every hour using the eqn (5) until equilibrium. First of all, from the swelling step, it can be noticed that for both thermo-sensitive copolymers the water content at the equilibrium remains relatively high for hydrogels. Despite the lower water solubility of PiPrOx, the PiPrOx-*net*-PAM copolymers lead to hydrogels with 1300 and 765% of water uptake for both 1/5 and 5/1 ratio respectively. Nevertheless, a slight opacity can be detected on fabricated cylinders for the PiPrOx containing hydrogels, which is due to the lower solubility of PiPrOx than PNIPAM in water (Fig. S4, ESI†). In consequence, water uptake of PMOx-*net*-PNIPAM reach 2100% for the ratio 1/5 and 1620% for the ratio 5/1.

As observed by the swelling assays, hydrogels with 5 molar excess hydrophilic units (PiPrOx$_{20}$-*net*-PAM$_{100}$ and PMOx$_{20}$-*net*-PNIPAM$_4$) did not show any change in swelling behavior with increasing temperature despite the presence of PiPrOx or PNIPAM (Fig. 4). Once the equilibrium swelling degree was
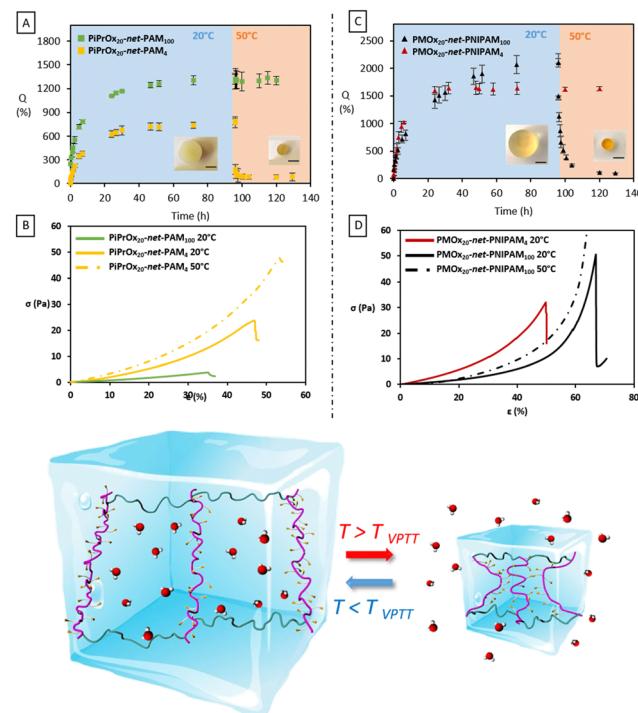
reached at 20 °C, no water release was observed once the temperature was increased, and the water content remained constant at 1630 and 1300% for PMOx$_{20}$-*net*-PNIPAM$_4$ and PiPrOx$_{20}$-*net*-PAM$_{100}$ respectively. This confirms again that the proportion of LCST segments is insufficient to generate a thermo-sensitive hydrogel. In contrast, for the hydrogels having 5 times molar excess of the thermo-sensitive moieties (PMOx$_{20}$-*net*-PNIPAM$_{100}$ and PiPrOx$_{20}$-*net*-PAM$_4$), the thermo-sensitivity is clearly visible (Fig. 4).

On the other hand, the thermo-response of the hydrogels containing a 5-molar excess of thermo-sensitive units to hydrophilic unis can be clearly observed. After 24 h incubation at 50 °C, PMOx$_{20}$-*net*-PNIPAM$_{100}$ hydrogels release 95% of the water to reach a swelling degree of 106%. Whereas, PiPrOx$_{20}$-*net*-PAM$_4$ hydrogels released 88% of their water to reach a 85% swelling degree after 24 h incubation at 50 °C. The water expulsion is translated in a significant collapse of the hydrogel volume by 60% after 24 h for both thermo-sensitive systems. Moreover, the contraction/expansion effect was successfully tested for 5 cycles.

The different macromolecular networks generated by both thermo-responsive hydrogels led to diverse swelling rates, we therefore investigated the mechanism of water diffusion at 20 °C using the Ritger–Peppas model (Fig. S5, ESI†).[42] The hydrogels of PMOx$_{20}$-*net*-PNIPAM$_{100}$ obeys the Fickian diffusion mechanism with a diffusional exponent constant n bellow 0.5 (n = 0.43). Conversely, for the copolymer PiPrOx$_{20}$-*net*-PAM$_4$ with a constant n at 0.6 clearly does not obey the Fickian diffusion mechanism, probably due to the lower solubility of POx moieties.

Mechanical properties under compression were evaluated on the cylinders obtained by the stereolithography process with a series of compressive measurements at 20 and 50 °C. From Fig. 4, the Young's modulus (E), the stress (σ_{max}) and the strain (ε_{max}) at break were deduced. For the thermo-responsive hydrogels, the Young's modulus slightly increases at 50 °C. The Young's modulus of $PiPrOx_{20}$-*net*-PAM_4 and $PMOx_{20}$-*net*-$PNIPAM_{100}$, estimated at 21.4 and 5.8 kPa at 20 °C increased at 50 °C to reach 23 and 6 kPa, respectively (Fig. 4). The notable improvement of the mechanical properties can be seen by the elongation at break and the stress at rupture. For $PiPrOx_{20}$-*net*-PAM_4, above the VPTT (at 50 °C) the 3D printed hydrogels broke at 55% elongation under a 45.5 kPa stress whereas below the VPTT (at 20 °C) the hydrogels broke at 40% deformation under a 24 kPa load. A similar improvement is also observed for $PMOx_{20}$-*net*-$PNIPAM_{100}$ hydrogels, where above the VPTT the hydrogels did not even break even after 80% deformation when at 20 °C the rupture occurred at 60% deformation under a 40 kPa load.

This improvement in the mechanical properties is due to the volume contraction of the hydrogels above the VPTT leading to a denser network reinforcing the polymer–polymer interactions and chain movement. This mechanical study on the hydrogels puts in relevance the thermal effect that induce a drastic volume change while improving the mechanical properties of the system.

3.4. 4D printing hydrogel by stereolithography

To evaluate the potential in 4D printing of the thermo-sensitive systems, we developed a device representative of the contraction/expansion effect under temperature change. Hence, a "bead trap" device composed of nine cubic cages of 5 mm sides and 1 mm of strut thickness was fabricated by SLA using $PiPrOx_{20}$-*net*-PAM_4 (Fig. 5B and Fig. S6, ESI†) and $PMOx_{20}$-*net*-$PNIPAM_{100}$ resins (Fig. 5C). Despite the thin sharpness of the backbone, the devices were perfectly manufactured by SLA with good mechanical handling for both hydrogels (Movies S1 and S2, ESI†). The next step was to demonstrate the thermal-stimulation impact on these 3D manufactured structures. As demonstrated with the $PMOx_{20}$-*net*-$PNIPAM_{100}$ system (Fig. 5C), the 3D structures showed an important swelling effect below the transition temperature at 20 °C, leading to a 6% increase in the cage dimensions. In contrast, when the temperature increases above the VPTT at 50 °C, the network collapses leading to a 70% shrinkage of the device's dimensions. This phenomenon of volume contraction on 3D structures makes it possible to illustrate this performance on the trapping of golden beads with a diameter of 2.2 mm (Fig. 5C). Thus, at 50 °C, the cages of the device are smaller than the diameter of the beads, which prevents them from falling into the cages. On the other hand, once the temperature has dropped to 20 °C, the device expands, allowing the beads to gradually enter in the cages. On returning to 50 °C, the beads are trapped by volume retraction of the device which causes a reduction in the size of the cages and becomes lower than the diameter of the beads. The reverse effect was showed in a movie on ESI† (Movie S3),
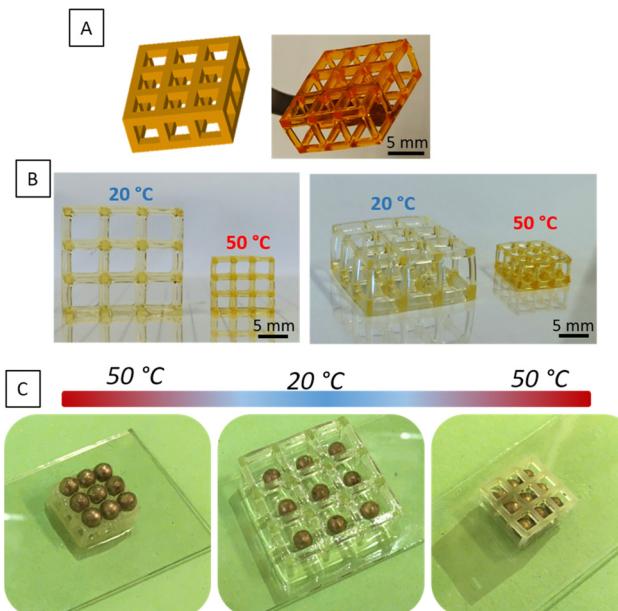
Fig. 5 (A) STL file of the "bead trap" and picture of the fabricated device by SLA just after printing with $PiPrOx_{20}$-*net*-PAM_4. (B) View of the volume shrinking above the VPTT for $PiPrOx_{20}$-*net*-PAM_4. (C) Proof of concept of the "bead trap" design below and above the VPTT using the hydrogel $PMOx_{20}$-*net*-$PNIPAM_{100}$.

where the beads are released from the device by changing the bath temperature, within 5 minutes. The trapping bead test has been demonstrated on the PiPrOx-*net*-PAM device on the Fig. S6 (ESI†), where the beads can pass through the device at 20 °C while the beads cannot cross the cage at 50 °C.

With a transition temperature close to the body temperature, these materials can find great interest in biomedical applications. As reported in several reviews, biomedical devices related to 4D printing have gain a growing interest in minimal surgeries or reaching cavities which are not accessible by traditional approaches.[43,44]

Hence, we fabricated a porous cylindrical stent using the thermo-sensitive $PiPrOx_{20}$-*net*-PAM_4 copolymer. As expected, the printed device undergoes the similar behavior of contraction with increasing temperature above the VPTT (Fig. 6). The diameter of the device decreases from 1.7 to 0.7 cm after shrinkage.

Besides the shape-morphing changes generated by the water expulsion from the hydrogel, such remarkable thermo-responsive
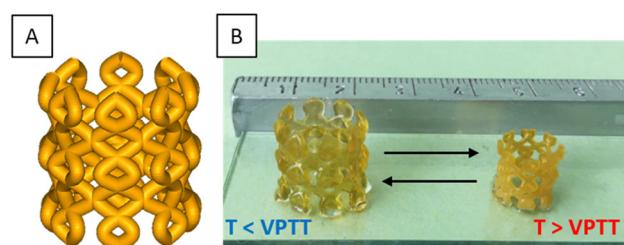
Fig. 6 (A) CAD model of a porous cylindrical stent. (B) Picture of the printed devices by SLA using $PiPrOx_{20}$-*net*-PAM_4 copolymer and showing the contraction of the stent device above and under the VPTT.

behavior can have great interest in controlled drug delivery, where a trigger release of bioactive molecules can be stimulated by the temperature.[45,46]

One of the major progresses of this study lies in the potential solution of PNIPAM substitution by the PiPrOx. Indeed, the POx hydrogels have been already demonstrated to not be toxic for cells and can even be used as resin for bioprinting.[17,18] The PiPrOx$_{20}$-net-PAM$_4$ showed an efficient thermo-responsive performance, which may pave the way towards more investigation of these thermo-responsive hydrogels in 4D printing.

4. Conclusion

In this first investigation on thermoresponsive hydrogels based on copolymers of poly(oxazoline) and poly(acrylamide), we succeeded to develop 4D printed devices with reversable shape morphing around body temperature. Two different types of hydrogels with diverse macromolecular networks were built, one with PiPrOx as thermo-responsive segments and the other with PNIPAM.

For the thermo-responsive hydrogels, a distinct contrast in water sorption was detected at the volume phase transition temperature, which consequently impacts the mechanical properties of the hydrogels. The contraction and expansion effect under temperature-change was illustrated by the 3D printed devices using SLA process which were capable of trapping and releasing beads upon thermal stimulation. Such contraction behavior around the body temperature leads to considerable potential to use such thermo-responsive hydrogels as a building block for biomedical devices.

Author contributions

T. Brossier: formal analysis; investigation; writing original draft. M. Habib: formal analysis; investigation; writing original draft. B. T. Benkhaled: formal analysis; investigation; writing original draft. G. Volpi: project administration; ressources; V. Lapinte: conceptualization; supervision; methodology. S. Blanquer: conceptualization; supervision; methodology; writing editing.

Conflicts of interest

There are no conflicts to declare.

Acknowledgements

References

1 Z. U. Arif, M. Y. Khalid, A. Zolfagharian and M. Bodaghi, *React. Funct. Polym.*, 2022, **179**, 105374.

2 D. J. Jiao, Q. L. Zhu, C. Y. Li, Q. Zheng and Z. L. Wu, *Acc. Chem. Res.*, 2022, **55**, 1533–1545.

3 Q. Y. Peng, J. S. Chen, T. Wang, X. W. Peng, J. F. Liu, X. G. Wang, J. M. Wang and H. B. Zeng, *InfoMat*, 2020, **2**, 843–865.

4 A. Bratek-Skicki, *Appl. Surf. Sci. Adv.*, 2021, **4**, 100068.

5 S. Pardeshi, F. Damiri, M. Zehravi, R. Joshi, H. Kapare, M. K. Prajapati, N. Munot, M. Berrada, P. S. Giram, S. Rojekar, F. Ali, M. H. Rahman and H. R. Barai, *Polymers*, 2022, **14**, 3126.

6 P. Imrie and J. Y. Jin, *J. Polym. Sci.*, 2022, **60**, 149–174.

7 M. Champeau, D. A. Heinze, T. N. Viana, E. R. de Souza, A. C. Chinellato and S. Titotto, *Adv. Funct. Mater.*, 2020, **30**, 1910606.

8 M. T. Hua, D. Wu, S. W. Wu, Y. F. Ma, Y. Alsaid and X. M. He, *ACS Appl. Mater. Interfaces*, 2021, **13**, 12689–12697.

9 L. Klouda, *Eur. J. Pharm. Biopharm.*, 2015, **97**, 338–349.

10 M. C. Koetting, J. T. Peters, S. D. Steichen and N. A. Peppas, *Mater. Sci. Eng., R*, 2015, **93**, 1–49.

11 L. Tang, L. Wang, X. Yang, Y. Y. Fen, Y. Li and W. Feng, *Prog. Mater. Sci.*, 2021, **115**, 100702.

12 J. Liu, L. Jiang, S. R. He, J. Zhang and W. Shao, *Chem. Eng. J.*, 2022, **433**, 133496.

13 M. J. Ansari, R. R. Rajendran, S. Mohanto, U. Agarwal, K. Panda, K. Dhotre, R. Manne, A. Deepak, A. Zafar, M. Yasir and S. Pramanik, *Gels*, 2022, **8**, 454.

14 K. Nagase, M. Yamato, H. Kanazawa and T. Okano, *Biomaterials*, 2018, **153**, 27–48.

15 A. S. Wadajkar, B. Koppolu, M. Rahimi and K. T. Nguyen, *J. Nanopart. Res.*, 2009, **11**, 1375–1382.

16 T. R. Dargaville, J. R. Park and R. Hoogenboom, *Macromol. Biosci.*, 2018, **18**, 1800070.

17 M. S. Haider, T. Ahmad, M. S. Yang, C. Hu, L. Hahn, P. Stahlhut, J. Groll and R. Luxenhofer, *Gels*, 2021, **7**, 78.

18 T. Brossier, B. T. Benkhaled, M. Colpaert, G. Volpi, O. Guillaume, S. Blanquer and V. Lapinte, *Biomater. Sci.*, 2022, **10**, 2681–2691.

19 S. N. Mahand, S. Aliakbarzadeh, A. Moghaddam, A. S. Moghaddam, B. Kruppke, M. Nasrollahzadeh and H. A. Khonakdar, *Eur. Polym. J.*, 2022, **17**, 111484.

20 T. Wloka, S. Czich, M. Kleinsteuber, E. Moek, C. Weber, M. Gottschaldt, K. Liefeith and U. S. Schubert, *Eur. Polym. J.*, 2020, **122**, 109295.

21 S. Czich, T. Wloka, H. Rothe, J. Rost, F. Penzold, M. Kleinsteuber, M. Gottschaldt, U. S. Schubert and K. Liefeith, *Molecules*, 2020, **25**, 5066.

22 S. Jana and M. Uchman, *Prog. Polym. Sci.*, 2020, **106**, 101252.

23 S. Huber and R. Jordan, *Colloid Polym. Sci.*, 2008, **286**, 395–402.

24 T. J. Li, H. Tang and P. Y. Wu, *Soft Matter*, 2015, **11**, 1911–1918.

25 M. Madau, G. Morandi, C. Rihouey, V. Lapinte, H. Oulyadi, D. L. E. Cerf, V. Dulong and L. Picton, *Polymer*, 2021, **230**, 124059.

26 M. Madau, G. Morandi, V. Lapinte, D. Le Cerf, V. Dulong and L. Picton, *Polymer*, 2022, **244**, 124643.

27 D. Han, Z. C. Lu, S. A. Chester and H. Lee, *Sci. Rep.*, 2018, **8**, 1963.

28 J. H. Guo, R. R. Zhang, L. N. Zhang and X. D. Cao, *ACS Macro Lett.*, 2018, **7**, 442–446.

29 M. N. I. Shiblee, K. Ahmed, M. Kawakami and H. Furukawa, *Adv. Mater.*, 2019, **4**, 1900071.

30 F. M. Cheng, H. X. Chen and H. D. Li, *J. Mater. Chem. B*, 2021, **9**, 1762–1780.

31 V. Mair, I. Paulus, J. Groll and M. Ryma, *Biofabrication*, 2022, **14**, 025019.

32 T. X. Viegas, M. D. Bentley, J. M. Harris, Z. F. Fang, K. Yoon, B. Dizman, R. Weimer, A. Mero, G. Pasut and F. M. Veronese, *Bioconjugate Chem.*, 2011, **22**, 976–986.

33 C. Noe, C. Tonda-Turo, A. Chiappone, M. Sangermano and M. Hakkarainen, *Polymers*, 2020, **12**, 1359.

34 M. Zanon, A. Chiappone, N. Garino, M. Canta, F. Frascella, M. Hakkarainen, C. F. Pirri and M. Sangermano, *Mater. Adv.*, 2022, **3**, 514–525.

35 T. Ogoshi and Y. Chujo, *Polymer*, 2006, **47**, 4036–4041.

36 T. R. Dargaville, R. Forster, B. L. Farrugia, K. Kempe, L. Voorhaar, U. S. Schubert and R. Hoogenboom, *Macromol. Rapid. Commun.*, 2012, **33**, 1695–1700.

37 L. Simon, N. Marcotte, J. M. Devoisselle, S. Begu and V. Lapinte, *Int. J. Pharmaceut.*, 2020, **585**, 119536.

38 J. Zhao, R. Hoogenboom, G. Van Assche and B. Van Mele, *Macromolecules*, 2010, **43**, 6853–6860.

39 H. Guo, A. Brulet, P. R. Rajamohanan, A. Marcellan, N. Sanson and D. Hourdet, *Polymer*, 2015, **60**, 164–175.

40 D. K. Taylor, F. L. Jayes, A. J. House and M. A. Ochieng, *J. Funct. Biomater.*, 2011, **2**, 173–194.

41 C. Benoit, S. Talitha, F. David, S. Michel, S. J. Anna, A. V. Rachel and W. Patrice, *Polym. Chem.*, 2017, **8**, 4512–4519.

42 P. L. Ritger and N. A. Peppas, *J. Controlled Release*, 1987, **5**, 23–26.

43 T. Agarwal, S. Y. Hann, I. Chiesa, H. T. Cui, N. Celikkin, S. Micalizzi, A. Barbetta, M. Costantini, T. Esworthy, L. G. Zhang, C. De Maria and T. K. Maiti, *J. Mater. Chem. B*, 2021, **9**, 7608–7632.

44 S. Malekmohammadi, N. S. Aminabad, A. Sabzi, A. Zarebkohan, M. Razavi, M. Vosough, M. Bodaghi and H. Maleki, *Biomedicines*, 2021, **9**, 1537.

45 D. Qureshi, S. K. Nayak, S. Maji, A. Anis, D. Kim and K. Pal, *Eur. Polym. J.*, 2019, **120**, 49–60.

46 S. Zu, Z. Wang, S. Zhang, Y. Guo, C. Chen, Q. Zhang, Z. Wang, T. Liu, Q. Liu and Z. Zhang, *Mater. Today Chem.*, 2022, **24**, 100789.